A New Model-Based Rotation and Scaling-Invariant Projection Algorithm for Industrial Automation Application

Huang-Chia Shih, *Member, IEEE*, and Kuan-Chun Yu

***Abstract*—This paper describes a simple approach for model-based template matching, which is robust to undergo rotation and scaling variations. An efficient image warping scheme spiral aggregation image (SAI), which has been utilized in this paper, provides a method for generating projection profiles for matching. In addition, it determines the rotation angle and is invariant to scale changes. The proposed spiral projection algorithm (SPA) for template matching enables the simultaneous representation for each value of projection profile, obtained through SAI, and provides structural and statistical information on the template. The experimental evaluation shows that the proposed SPA achieves very attractive results for template matching in the industrial automation application.**

***Index Terms*—Image warping, industrial automation, rotation invariant, scale invariance, template matching.**

I. Introduction

STATE-of-the-art research in machine vision techniques in industrial applications has been successfully implemented in such area as inspection system [1]–[3], robotic vision systems [4], [5], autonomous vehicle navigation [6]–[10], and recognition system [11], [12]. Template matching is a critical technique in numerous visual-based pattern recognition applications. To cope with the template undergoing unpredictable geometric transformations, it is not surprising that the use of the invariant local descriptor is indispensable. Frequently, template matching suffers from such problems in rotation, scaling, translation, and brightness/contrast changes. Conventional approaches are seldom able to handle these problems simultaneously, depending on the model.

Generally speaking, template matching algorithms are classified into projection-based and transformation-based methods. The projection-based method focuses on extracting the intrinsic characteristics from a particular sampling model or projection path. The local structural information of the template can be preserved and enhanced using an appropriate descriptor that is insensitive to geometric transformations. For instance, the radial projection [13] is a sampling method from two-dimensional (2-D) image pixels under radial lines into a one-dimensional (1-D) profile as a function of the radial line angle. The 1-D profile obtained from the radial projection is normally invariant to scale changes. In addition, the ring projection [14]–[18] is a simple algorithm that enables transforming 2-D patterns into 1-D profiles by circularly aggregating pixels on the same radius from the center point, in order to achieve rotation-invariant features. One of the most capable schemes for dealing with both rotation and scale-invariant properties is based on the cascade model. Kim and Araujo [19] showed that a cascade framework that ring projection method was used to deal with the rotation variation and that the radial projection method was applied to estimate the local rotation angle.

On the other hand, the transformation-based framework converts the spatial image plane to the feature plane using transformation methods. Furthermore, combining the projection-based and transformation-based scheme has been considered in [20]–[22]. Apparently, the fusion framework significantly increased the complexity of the system but was still unable to deal with the serious geometric changes. Thus, we focused on modeling the image directly in the spatial domain and recovered the best rotation and scaling by performing a correlation on tiles that were projected into feature coordination called spiral aggregation image (SAI). We concentrated on solving the geometric variability due to the change in pose and the different angle of the viewpoint by using a single projective model called spiral projection algorithm (SPA).

In this paper, a projection-based grayscale template matching is proposed to understand more structural information from the template and to remove the computational burden from the transformation cost. As mentioned earlier, the projection-based approach such as the ring and radial projection methods, although they show promising results in experiments, has some unsolvable drawbacks. Although profiles of the ring projection method for object search have been used numerously for rotation-invariant template matching [16], [23], [24], they are not applicable in some situations, such as when the template has a circular symmetrical pattern with a radial appearance in a particular orientation such as a clock, compass, color wheel, and so on. In addition, each value of the projection profile is collected from a different number of sampling pixels, which is a function of the radius. In other words, the spatial resolution sampling from the inner circle must be less than that of the outer circle. Each value of the projection profile is acquired from a different number of sampling pixels. However, it is very

Manuscript received June 6, 2014; revised May 5, 2015; accepted June 25, 2015. Date of publication March 16, 2016; date of current version June 9, 2016. This work was supported in part by the Ministry of Science and Technology of Taiwan under Grant MOST 103-2221-E-155-027-MY2.

The authors are with the Department of Electrical Engineering, Human–Computer Interaction Multimedia Laboratory, Yuan Ze University, Taoyuan 32003, Taiwan (e-mail: hcshih@saturn.yzu.edu.tw; d917904@oz.nthuedu.tw).

Color versions of one or more of the figures in this paper are available online at http://ieeexplore.ieee.org.

Digital Object Identifier 10.1109/TIE.2016.2543178

difficult to provide an equivalent sampling resolution for each of the values, making it impossible to accurately handle the overall error model.

The remainder of this paper is organized as follows. Section II presents the proposed algorithm: spiral projection and the image warping method that is robust to rotation and scaling invariance. Experimental results are provided in Section III and finally we discuss our findings and draw our conclusion in Section IV.

II. Algorithm

A novel projection algorithm for robust template matching is developed in this study. This algorithm is a model-based projection scheme, sampling pixels by using the spiral expansion model for both the template and the test subimage. Based on the characteristics of spiral expansion, the sample evolution included both horizontal and vertical displacements simultaneously.

A. Spiral Projection Algorithm

According to the definition of Archimedean spirals [25], a continuous spiral trajectory can be described as

$$\rho_{\emptyset} = \alpha\emptyset, \quad 0 \leq \emptyset < \infty \tag{1}$$

where α denotes a constant describing the radial distance in a polar coordinate system, and $\rho_{\emptyset}$ is the distance from the point on the spiral line to the origin with the corresponding angle $\emptyset$. The trajectory can be formed as $\emptyset = 2\pi c + \omega$, where $c \in \mathbb{Z}$ indicates the number of laps, and ω is the angle of the x-axis in the Cartesian plane, which can act as the angular velocity, periodically rotating with the origin point. To align the origin of the spiral trajectory with the Cartesian coordinate, we designed $\emptyset = 2\pi k$, where k denotes the number of laps, and $k \in \mathbb{R}$ in order to satisfy the requirement of the noninteger laps. Thus, the spiral line can be transformed onto the Cartesian plane

$$\begin{cases} u_{\emptyset} = \alpha\emptyset\cos\emptyset, \\ v_{\emptyset} = \alpha\emptyset\sin\emptyset, \end{cases} \quad 0 \leq \emptyset < \infty. \tag{2}$$

In order to deal with the scaling variation, we attempted to design a similar spiral line regardless of the size of the test subimage. This provided a consistent sampling path from the point of origin (u_0, v_0) to the boundary of the image. The intrinsic texture features were preserved by the stationary sampled points on the reference template and test subimage. Consequently, it was important that the number of cycles after a certain evolution time remained unchanged. Fig. 1 shows a graphical illustration of the spiral sampling model. Let us consider two points (ρ, $\emptyset$) and (ρ', $\emptyset + 2\pi$) that are located in the same angle. If we apply for (1), then we have $\rho = \alpha\emptyset$, $\rho' = \alpha(\emptyset + 2\pi)$, and $d = |\rho - \rho\prime| = 2\pi\alpha$. Let d denote the smallest radial distance (i.e., radial interval) between these two points.

Suppose that the size of the image is $N \times N$, and K denotes the maximum number of laps from the point of origin to the boundary point, which is used to restrict the evolution of the spiral span. Let $\rho_{\max}$ denote the farthest point from the point of origin on the spiral line that equals $N/2$, so that

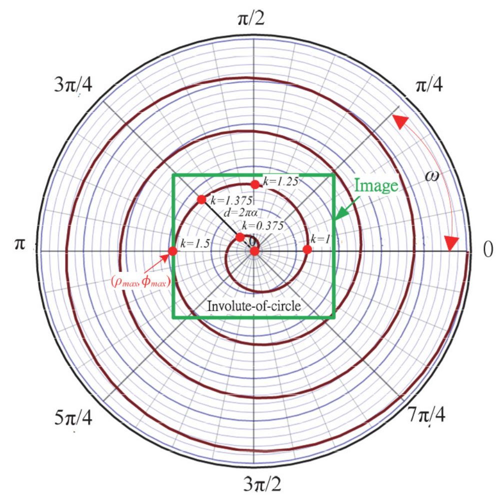

Fig. 1. Illustration of the spiral sampling algorithm.

$$\rho_{\max} = dK = 2\pi\alpha K. \tag{3}$$

Substituting $\alpha = \rho_{\max}/2\pi K$ into (1) satisfies our requirement that the finite samples with the bound of expansion $\emptyset_{\max} = 2\pi K$. Thus, we obtain a time-limited spiral line in the polar plane

$$\rho_{\emptyset} = \alpha\emptyset, 0 \leq \emptyset < 2\pi K. \tag{4}$$

Based on the time-limited spiral function, we have a sample location (u_i , v_i) in the Cartesian plane

$$\begin{cases} u_i = \alpha\emptyset_i\cos\emptyset_i, \\ v_i = \alpha\emptyset_i\sin\emptyset_i, \end{cases} \quad 0 \leq \emptyset_i < 2\pi K \tag{5}$$

where $\emptyset_i$ denotes the corresponding angle arranged on $[0, \emptyset_{\max})$.

In the digital image, we need to find discrete samples along the spiral trajectory. A discrete approximation of the sample pixels along a spiral trajectory is given by the predefined K and the size of the image. Let $\boldsymbol{S}$ denote the collection of the spiral samples along the spiral trajectory from the reference template $T(u, v)$, expressed as

$$\boldsymbol{S} \triangleq \{s_i\}|_{i=1\sim P} = \bigcup_{i=1}^{P} T(u_i, v_i) \tag{6}$$

where P denotes the amount of sampling points. The angular interval ω_j of the jth sample can be computed as follows:

$$\omega_j = \left(\frac{\theta_{\max}}{P}\right) * j \tag{7}$$

where j denotes the sample index.

We defined a single spiral curve in (1), i.e., $\rho_{\emptyset}$, where $0 \leq \emptyset < \infty$ in polar plane. Here, we constructed a projection model based on the spiral sampling. Each value of the projection profile is obtained by aggregating all of the pixels in the spiral curve. Suppose $T(u,v)$ is a template image with size $N \times N$ in the Cartesian plane, then the pixels on the spiral curve sample can be written as

$$\{s_n\}|_{n=1\sim P} \triangleq \rho_\emptyset = T\left(u\left(\omega_n\right), v\left(\omega_n\right)\right), \quad 0 \le \omega_n < \theta_{\max} \text{ and } n = 1, 2, 3, \ldots, N \tag{8}$$

where

$$\begin{cases} u(\cdot) = \alpha\omega_n \cos\omega_n \\ v(\cdot) = \alpha\omega_n \sin\omega_n \end{cases} \tag{9}$$

where $\alpha\omega_n$ is controlled by the number of laps K. Assume that we need to rotate the spiral line via the center of the template. Using the geometric rotation operation to transform the pixel locations (u, v) from the input image to (u', v') in the output image, then the new sampling points with clockwise rotating of angle φ are expressed by

$$\begin{cases} u'(\cdot) = u \cos\varphi - v \sin\varphi \\ v'(\cdot) = u \sin\varphi + v \cos\varphi. \end{cases} \tag{10}$$

By replacing u and v in (10) by (9), we obtain

$$\begin{cases} u'(\cdot) = \alpha\omega_n \cos\omega_n \cos\varphi - \alpha\omega_n \sin\omega_n \sin\varphi \\ v'(\cdot) = \alpha\omega_n \cos\omega_n \sin\varphi + \alpha\omega_n \sin\omega_n \cos\varphi. \end{cases} \tag{11}$$

Using the compound angle formula

$$\begin{cases} u'(\cdot) = \alpha\omega_n(\cos\omega_n \cos\varphi - \sin\omega_n \sin\varphi) \\ \qquad = \alpha\omega_n \cos\left(\omega_n + \varphi\right) \\ v'(\cdot) = \alpha\omega_n\left(\cos\omega_n \sin\varphi + \sin\omega_n \cos\varphi\right) \\ \qquad = \alpha\omega_n \sin\left(\omega_n + \varphi\right) \end{cases} \tag{12}$$

where $0 \le \varphi < 2\pi$.

Consequently, the SAI of whole template is indexed by angle φ, which can be formulated as

$$\mathcal{P}^T\left(\varphi\right) = \left(\frac{1}{P}\right)\sum_{j=1}^{P} T[\alpha\omega_j \cos\left(\omega_j + \varphi\right), \alpha\omega_j \sin\left(\omega_j + \varphi\right)], \quad 0 \le \varphi < 2\pi. \tag{13}$$

Based on the definition of the Archimedean spiral, the appearance of a spiral curve does not change with the size of the image. The SAI is scaling invariant, and we can extract the desired projection profiles from it. In this paper, we simply used the mean value as the profile value. Let $\mathcal{P}_H$ denote the horizontal projection of the SAI, we have

$$\mathcal{P}_H\left(\varphi\right) = \left(\frac{1}{P}\right)\sum_{i=1}^{P} \mathrm{SAI}\left(i, \varphi\right). \tag{14}$$

In addition, if $\mathcal{P}_V$ denotes the vertical projection of the SAI, which is composed by the spiral inner-ring pixels indexed by i, then we have

$$\mathcal{P}_V\left(i\right) = \left(\frac{\Delta\varphi}{2\pi}\right)\sum_{\varphi=0}^{2\pi} \mathrm{SAI}\left(i, \varphi\right) \tag{15}$$

where $\Delta\varphi$ denotes the sampling offset in the rotation angle of spiral.

According to the characteristics of SAI, we can derive the projection profile using $\mathcal{P}^T\left(\varphi\right) = \mathcal{P}_H\left(\varphi\right)$, where $0 \le \varphi < 2\pi$. Similarly, the projection profile of the instance of the test subimage I_s with center location (x_s, y_s) is formed as

$$\mathcal{P}^{I_S(x_s,y_s)}\left(\varphi\right) = \left(\frac{1}{P}\right)\sum_{k=1}^{P} I_s\left[\left(x_s + d_x^k\right), \left(y_s + d_y^k\right)\right] \tag{16}$$

where (d_x^k, d_y^k) denotes the offset in the x- and y-directions along the spiral curve, which is computed by

$$\begin{cases} d_x^k = \alpha\omega_k \cos\left(\omega_k + \varphi\right), \\ d_y^k = \alpha\omega_k \sin\left(\omega_k + \varphi\right), \end{cases} \quad 0 \le \varphi < 2\pi. \tag{17}$$

The major goal of the algorithm is to model the reference template and use it to estimate the rotation angle of test subimage I_s with center location (x_s, y_s). Intuitively, the normalized correlation $\gamma\left(x_s, y_s\right)$ is used in the matching process to determine the similarity between the reference template and the test subimage with center location (x_s, y_s). The rotation angle φ^* can be determined by the offset τ, which produces the maximal normalized cross-correlation (NCC) value between the parametric template and test subimage as follows:

$$\varphi^* = \mathrm{argmax}_\tau \left\{\gamma\left(x_s, y_s\right), \tau\right\} \forall\tau \in \varphi \tag{18}$$

where

$$\gamma\left(x_s, y_s\right) \triangleq \mathcal{P}^T, \mathcal{P}^{I_S(x_s,y_s)} = \frac{\eta_s}{\parallel \mathcal{P}^T \parallel \cdot \parallel \mathcal{P}^{I_S} \parallel} \tag{19}$$

where denotes the l-2 norm distance, and η_s refers to the correlation between the reference template and the current test subimage, is defined as follows:

$$\eta_s = \sum_{\varphi=0}^{2\pi} \mathcal{P}^T\left(\varphi\right) \cdot \mathcal{P}^{I_S(x_s,y_s)}\left(\varphi\right). \tag{20}$$

B. Properties of the SAI

A constant-size feature map is constructed by collecting pixels from the original image regardless of the size of the image. The so-called SAI is created by the set of pixels on the spiral line with the corresponding angle from image space (u, v) to projection space (i, φ). Let $\mathrm{SAI}\left(i, \varphi\right)$ denote the feature map sampled from the pixels along the spiral line at a rotation of φ degrees, and i denotes the index of the pixel sample. Each group of sample pixels is vertically replaced into $\mathrm{SAI}\left(i, \varphi\right)$ according to their angle. As mentioned above, $i = 1 \sim P$, where P is the number of sample pixels on each spiral line. Assuming that the spatial resolution of the spiral line is $\Delta\varphi$ degrees, we have $2\pi/\Delta\varphi$ sets of samples on each spiral line, rotating at φ degrees. Therefore, we can obtain a feature map with a fixed size of $2\pi/\Delta\varphi$ by P.

A conceptual illustration of the SAI construction is shown in Fig. 2. We draw two spiral lines in $\varphi = 0°$ and π with blue and magenta star marks in Fig. 2(a). Each one is then sequentially arranged to the horizontal slice as shown in Fig. 2(b). Then, the horizontal and vertical profiles can be obtained as Fig. 2(c). To

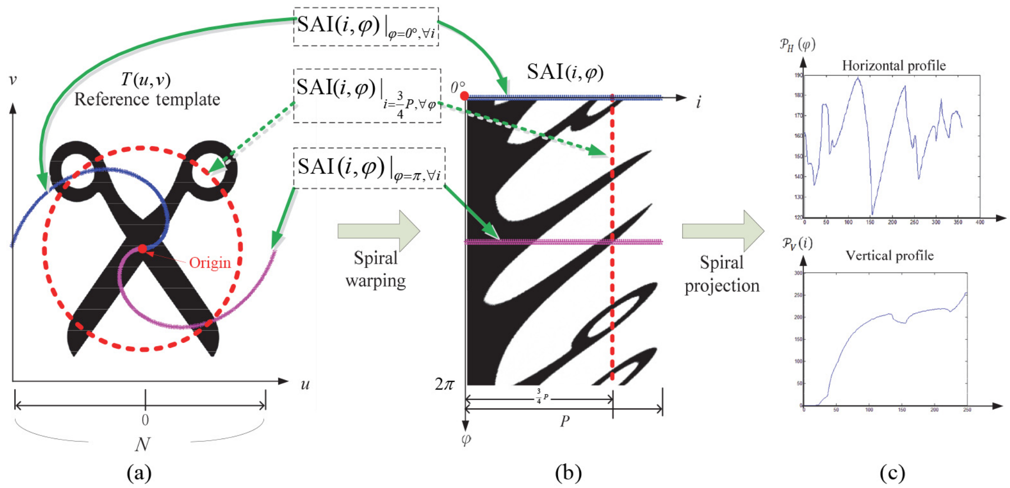

Fig. 2. Graphical illustration of the SAI, $K = 0.5$.

integrate all samples on each horizontal slice, we construct a spiral projection profile. The concentric circles with red dashed marks denote the samples with the same serial number *i* on each rotated spiral line. In the feature map, this is displayed on the vertical slice with position *i*. To integrate all samples on each vertical slice, we construct a spiral inner-ring projection profile.

In short, the SAI has two important properties: 1) It is scale-invariant: when the size of the test image changes, the horizontal and vertical projection profiles of SAI remain globally stationary. 2) It is rotation-distinguishable: if the image is rotated, it is reflected on the SAI by a vertical shift. The rotation angle can be determined by the vertical displacement of the feature map, and finding the maximal offset of the cross-correlation coefficient between the SAIs of the reference template and the test subimage.

C. Template Matching Using SPA

In this study, we aim to determine the position and orientation of the reference template T from each sampled subimage I_s from the test image.

The advantage of the SAI image is that scale changes do not affect the appearance of the SAI. Histogram equalization (HE) [26] is used to balance the local contrast variation between the template and the test subimage. The rotation performed in the original image will reliably respond to the SAI with vertical scrolling. Therefore, we attempted to solve the problems of scaling and rotation simultaneously.

From the vertical aspect, the scaling and rotation variations will not affect the vertical projection of the SAI. For a given test subimage, we first obtain $\mathcal{P}_V^{S(x_n,y_n)}(i)$ that forms the vector with 360 values (i.e., $\varphi = 0 - 2\pi$) on each candidate point n and the ith spiral inner-ring pixel by means of (15). When compared with the set of points on the reference template, i.e., $\mathcal{P}_V^T(i)$, the average error of each point is less than the predefined constant β_1, then the corresponding feature score is added. β_1 reflects the distinction between the mean of the spiral inner-ring projection on the test subimage and the reference template. Let $F_v(n)$ denote the integral similarity score of the nth test point from $L[s_n]$, in other words

$$F_V(n) = \sum_{i=0}^{P} u\left[\left|\mathcal{P}_V^{S(x_n,y_n)}(i) - \mathcal{P}_V^T(i)\right|, \beta_1\right] \tag{21}$$

where

$$u[A,B] = \begin{cases} 1 & \text{if} \quad A < B \\ 0 & \text{if} \quad A > B. \end{cases} \tag{22}$$

From the horizontal aspect, we can compute the horizontal projection $\mathcal{P}_H^{S(x_n,y_n)}(\varphi)$ of the test subimage and $\mathcal{P}_H^T(\varphi)$ from the reference template using (14). Substituting $\mathcal{P}_H^{S(x_n,y_n)}(\varphi)$ and $\mathcal{P}_H^T(\varphi)$ into (18)–(20), we find the best matched rotation angle φ^*. Based on the SAI characteristics, these two horizontal projections satisfy the shift relationship. Hence, we can obtain the horizontal similarity score

$$F_H(n) = \sum_{\varphi=0}^{2\pi} u\left[\left|\mathcal{P}_H^{S(x_n,y_n)}(\varphi+\varphi^*) - \mathcal{P}_H^T(\varphi)\right|, \beta_2\right] \tag{23}$$

where β_2 denotes a predefined constant reflecting the distinction between the mean of the horizontal projection on the test subimage and the reference template.

Finally, we sort the similarity score of both the vertical and the horizontal results. When the similarity scores F_v and F_H are both top-ranked, then the corresponding point will be preserved in L.

III. Performance Evaluation

To demonstrate the performance of the proposed algorithm to template matching, the experiments were performed with three different types of datasets.

A. Preliminary

For this study, we collected the templates from three datasets, as shown in Table I.

TABLE I
TESTING DATASETS IN THE EXPERIMENTS

	Instance images	Background images
Dataset-1: logos and badges		
	Instance images	Background images
Dataset-2: image patches	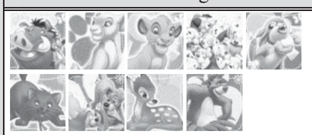	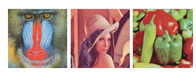
	Instance images	Background images
Dataset-3: PCB components		N/A, the instance images both are cropped from the original images

TABLE II
ABBREVIATIONS OF CORRUPTED NOISES FOR EVALUATION

Distortions	Abbreviations	Demonstrations
Illumination change	DI-10	Darken 10% of the intensity
	DI-20	Darken 20% of the intensity
	BI-10	Brighten 10% of the intensity
Contrast adjustment	DC-10	Depressed 10% of the contrast
	DC-15	Depressed 15% of the contrast
	EC-10	Enhanced 10% of the contrast
Noise corruption	GSF	*Gaussian smoothing filter* with 5x5 mask
	JPEG	*JPEG* compressed with 10% compression ratio
	SPN	Corrupted by *salt & pepper noise* with $p = 0.05$
	PN	Corrupted by *Poisson noise* with variance $= 0.5$

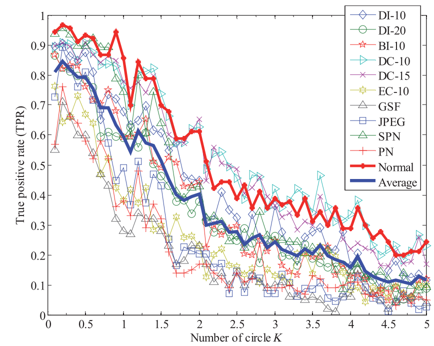

Fig. 3. True positive rate (TPR) of different illumination, contrast, and noise distortions for a varying number of circle *K*.

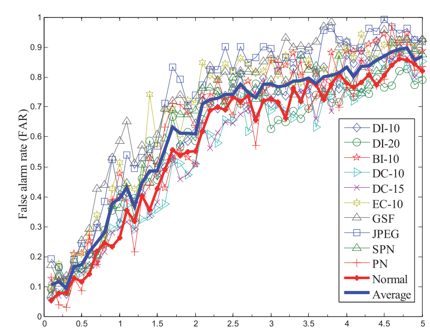

Fig. 4. False alarm rate (FAR) of different illumination, contrast, and noise distortions for a varying number of circle *K*.

1) Dataset-1: Logos and Badges: There were a total of 20 templates used in the evaluation of the system, 5 from the car logo, 12 from the university badge, and 3 from an official badge.

2) Dataset-2: Image Patches: Nine query templates were resized by scaling factors chosen randomly in the range [0.7 and 1.4], and pasted them in random nonoverlapping locations to form as eight test images, which collected from the source website of [27]: http://www.lps.usp.br/hae/software/forapro/. Using the rotation and scaling versions of the sample instances randomly embedded onto background images.

3) Dataset-3: PCB Elements: Images of circuit samples from e-book: 4 printed circuit board (PCB) images were used to crop 44 instances, including integrated circuit, capacitors, chipsets, switch, junctions, mercury batteries, etc. Nevertheless, some geometric deformations will be induced due to the capturing orientation. The minimum resolution among the instances was 15×12.

The reference template was first selected and its center position defined. Before the SPA can be utilized, the vertex samples must be restored from the SAI feature space with different scaling factors. This enables the system to generate robust feature descriptions for searching the sample instance of the test image and attack the rotation and scale deformation. The main purpose of template matching is to determine the accurate position and orientation of the template of the noise corrupted image.

B. Sensitivity Analysis of the Spiral Parameters

In the first experiment, we evaluated the sensitivity to distinguish the proposed SPA. In sampling the spiral model, the number of circles (i.e., *K*) in the spiral plays an important role in the degree of accuracy. Therefore, our aim was to test the sensitivity of the spiral parameter *K* using the rotation versions of the sample instances randomly embedded onto a cluttered background. As shown in Table II, the predefined illumination change, contrast adjustment, and noise corruption are employed to the *dataset-1: logos and badges*. All of the instance samples are set into a cluttered background image with random orientation and corrupted with different noise variations.

We tested the template matching performance of the proposed SPA. To investigate the sensitivity of the proposed algorithm to the spiral parameter, the detection was performed by varying the *K* parameter to test the image datasets for intensity, contrast transformation, and a variety of noise, all on a cluttered background. To quantitatively measure the sensitivity of the proposed method, the TPR and an FAR against the *K* values are shown in Figs. 3 and 4.

From Figs. 3 and 4, we can conclude that when the circle of the spiral increases, the accuracy of the template matching decays. Moreover, the error rate will increase at the same time. However, the circle of the spiral model (i.e., *K*) cannot shrink forever, and when K is selected to be less than 0.5, the true positive rate and the FAR will show a similar performance. If the amount of corrupted noise is substantial, then the accuracy of the system performance is compromised, especially when K is less than 0.1. Therefore, the best K will range between 0.2 and 0.5. Based on our observations, the system performs best for the TPR measurement when K is 0.2.

Nevertheless, the best performance for the FAR value is $K = 0.3$. In order to avoid missing the true instances, we applied $K = 0.3$ in the following experiments.

It is worth to discuss that the selection of the number of the laps K. When a large K is chosen, much of the uncorrelated information has been sampled in the spiral line. Hence, the less distinctive representations will be observed. In addition, a great number of noises could be sampled, it results in a significant increase of the false candidates are detected surrounding the true location. From a statistics view point, we observed the single spiral line over different K for each sample. A large K always performs worse due to the loss of intrinsic characteristics. Based on our observation, the variance of the entropy values will tend to small when a large K is used. It means that more undesired noise has been added, the same reason to the variance of homogeneity and contrast computations.

C. Robustness to the Rotation and Scaling Variations

To evaluate the robustness of the proposed method, a few vertex templates were created from the given reference template with different rotation angles and scaling factors with noise corruptions. In this experiment, two evaluations are demonstrated. For the first evaluation, we set $K = 0.3$ to test the robustness of the rotation-invariance. Three scaling factors {0.8, 1, and 1.5} were used to evaluate the robustness of scale changes.

In order to quantitatively measure the effectiveness of our proposed SPA for dealing with the rotation and scaling transformations, we applied two commonly used metrics of precision and recall to describe the performance of the template matching algorithm. They are defined as follows:

$$\text{Precision} = \frac{\text{TP}}{\text{TP} + \text{FP}}, \quad \text{Recall} = \frac{\text{TP}}{\text{TP} + \text{FN}} \tag{24}$$

where TP, FP, and FN denote true positive, false positive, and false negative, respectively. However, when the recall rate is high, it is difficult to achieve a high precision rate; conversely, if the precision rate is high, it is impossible to have a high recall rate. Consequently, we used the F-measure to evaluate the overall performance as follows:

$$F\text{-measure} = 2 \times \left(\frac{\text{precision} \times \text{recall}}{\text{precision} + \text{recall}}\right). \tag{25}$$

1) Rotation Invariance: In order to test the rotation-invariant property of the proposed SPA framework, we set $K = 0.3$ for finding the location and orientation of the instances. Fig. 5 shows the matching result using reference template as shown in Fig. 5(a). The corresponding center position and orientation are shown in Fig. 5(b). When SPA was used, four peaks of matching scores were obtained, as shown in Fig. 5(c).

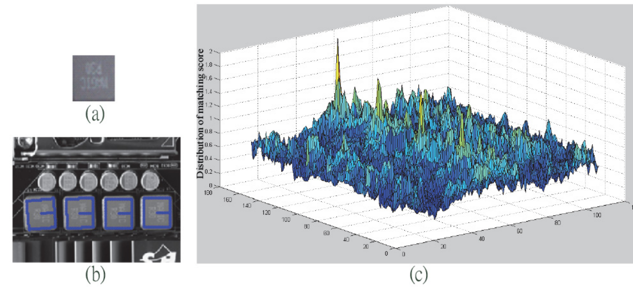

Fig. 5. Results of matching with the rotation variations. (a) Template image. (b) Detected patches with bounding box and orientation. (c) Matching scores (four peaks denote the center location of the instances).

TABLE III
MATCHING PERFORMANCE OF THE ROTATION VARIATIONS

Noise	# instances	TP	FP	FN	Precision (%)	Recall (%)	F-measure (%)
Normal	100	95	12	5	88.79	95.00	91.79
Contrast adjusted	300	245	43	55	84.97	81.67	82.94
Illumination changed	300	250	42	50	85.61	83.33	84.45
Noise corrupted	400	315	59	85	84.97	78.75	81.00
Totally/average	1100	905	156	195	85.59	82.27	83.45

We created 1100 instance samples and set into the corresponding background image with random orientation and corrupted with different noise variations. Using the F-measure is the only way to obtain a high performance that simultaneously has a high precision and high recall rates. As shown in Table III, the proposed method applied for test the image datasets without the addition of noise achieved a performance of 91.79% in the F-measure. The overall precision rate is not very sensitive to illumination and contrast changes, which is less than 5% of the overall precision rate. Overall, the proposed matching algorithm achieved a 84.97% precision rate and 78.75% recall rate when corrupted by the different noises. On average, it achieved a performance of 83.45% when the three types of image distortions were applied.

2) Scaling Invariance: In this experiment, three scaling factors {0.8, 1, and 1.5} were used to evaluate the robustness of scale changes. The vertex templates were generated based on the proposed image warping scheme. The same SAI images could be obtained for different scales of vertex templates. The resolution of the test image was 400×400. The vertex templates with accurate scale factors, rotation angles, and the positions for test set 1 (with $K = 0.3$) were all detected correctly.

In addition, we extended our experiment and tested the robustness for noise interference such as listed in Table II (e.g., change in intensity, contrast adjustment, lossy JPEG compression, and some kernel noises). Fig. 6 shows the results of the scale-invariance experiment for the normal sample and template. The number and the orientation of the bounding box denote the sign code and rotation angle of the detected instance. Table IV shows the performance of template matching with noise corruptions.

Fig. 6. Result of template matching for four templates of groups with rotation and scaling variations ($K = 0.3$).

TABLE IV
MATCHING PERFORMANCE OF THE SCALING VARIATIONS

Noise	# instances	TP	FN	Hit rate (%)
Normal	60	59	1	98.33
Contrast adjusted	180	159	21	88.33
Illumination changed	180	155	25	86.11
Noise corrupted	240	194	46	80.83
Totally/average	660	567	93	88.40

TABLE V
PERFORMANCE COMPARISON OF THE SPIRAL PROJECTION AND RADIAL PROJECTION

	Spiral			Radial		
Lines	Precision (%)	Recall (%)	*F*-measure (%)	Precision (%)	Recall (%)	*F*-measure (%)
5	49.5	41.3	45.7	52.5	18.5	33.2
10	79.6	74.9	77.0	84.6	40.5	61.6
15	91.4	91.7	91.5	91.6	62.5	79.3
20	94.8	98.3	96.2	96.6	73.7	87.9
25	96.0	98.9	97.4	96.5	79.1	88.8
30	97.0	99.0	97.8	97.0	86.6	90.6
35	97.0	99.4	98.0	97.0	90.6	92.5
40	97.0	100.0	98.2	97.0	97.8	94.5
Average	87.79	87.94	87.73	89.10	68.66	78.55

E. Comparison With Radial Projection Method

As aforementioned, a radial projection is a kind of extreme case of spiral projection. However, spiral projection method reserved more orientation information and texture properties about the image. In this section, we have conducted an experiment to demonstrate the accuracy using a particular number of radial and spiral sampling lines. More specifically, a part of spiral lines among 360° would be used to represent the template. Table V shows the comparison between spiral and radial projection methods using recall, precision, and F-measure indexes. This demonstrates that the recall rate of radial projection was significantly lower than it of spiral projection, especially when a small number of spiral lines were adopted. According to the result of F-measure evaluation, the spiral projection method outperforms the radial projection algorithm about 10% in accuracy. Except of more spiral lines being used, it is because that the more chaos will be induced unexpectedly. As well, the number of sampling lines reflects the execution time. Consequently, it can be treated as a tradeoff problem between computational cost and detection accuracy.

Fig. 7. Results of SPA using the dataset-2 from [27], where $n_s = 8$ and $n_c = 1$.

TABLE VI
COMPARISON BETWEEN THE *SPA* AND *Forapro-NCC*

Dataset-3	SPA			Forapro-NCC [27]		
Errors (maximum = 44)	$n_c = 10$	$n_c = 20$	$n_c = 45$	$n_c = 10$	$n_c = 20$	$n_c = 45$
$n_s = 4$	8	6	6	17	11	9
$n_s = 5$	6	5	4	14	8	4
$n_s = 6$	5	3	1	12	7	3
$n_s = 8$	5	0	0	9	4	3

F. Comparison of State-of-the-Art Method and Datasets

Previous studies have examined that the template matching algorithms can be divided into two groups: projection-based and transformation-based approaches. Recently, the growth of research trends has focused on the hybrid approach. For example, *Forapro* (Fourier coefficients of radial projections) [27] is an efficient template matching approach. It uses the radial and circular features to detect the matching candidates.

The NCC is used to decide whether each of matching candidates is a true or false matching result. Another possible filtering method is based on the generalized Hough transform [28]. However, it requires a set of stable subtemplates providing to against the partial occlusions. For the purpose of fairness, we compare our method only with the *Forapro-NCC* method.

We repeated the experiment of scale changes using the dataset in [27], including 24 memory game cards with 12 different figures. In this experiment, the *dataset-3: PCB components* were applied for evaluations. This dataset for testing the template matching algorithm is more challenging due to the high-corrupted background and greater scale factor ranges. In the beginning, nine query templates were resized by scaling factors chosen randomly in the range [0.7 and 1.4], and pasted them in random nonoverlapping locations to form as eight test images. Fig. 7 shows the matching results including the rotation-scaling variations. Table VI depicts the number of observed errors using the *Forapro-NCC* and the proposed method, varying the number of candidate pixels n_c and the number of scales n_s. According to the results of Table VI, the proposed algorithm is capable of scale variations. To localize the template locations in the test image, the SPA outperforms the *Forapro-NCC* method. For example, the number of matching candidates n_c represents the matching tolerance of the location offset. When a smaller value of n_c being assigned, it needs to search a pixel location more precisely. Based on our observations, with the same condition, i.e., $n_c = 10$, our method obtains less errors than *Forapro-NCC* method.

IV. Conclusion

In this paper, we proposed a theoretically and computationally simple approach that is sufficiently robust to undergo rotation and scaling variations and can be applied for realistic visual template matching application. A simple and well-defined feature map, the proposed SAI is illustrated to deal simultaneously with the rotation- and scaling-invariance transformation. The scale changes do not affect the appearance of the SAI. The rotation performed in the original image faithfully responds to the SAI when scrolled vertically. More specifically, when the original image suffers from a counter-clockwise rotation, the SAI rotates downward. Similarly, if a clockwise rotation occurs, the SAI rotates upward. The proposed SPA that provides structural and statistical information on the template in a more general and easier to comprehend format is presented here. Compared to the ring projection method, the spiral-based projection provides a high level of sensitivity and scanning efficiency. As well, the inherent spatial information will be better preserved than by using the radial projection algorithm. Many prospective applications are possibly addressed such as automated industrial inspections, vision-based defect detection, object modeling, and industrial automation applications. As long as the reference template is provided, the proposed SAI can be used to construct a robust model library. It not only enables to attack the rotation variations but also performs to attack the scaling variations.

References

[1] A. Kumar, "Computer-vision-based fabric defect detection: A survey," *IEEE Trans. Ind. Electron.*, vol. 55, no. 1, pp. 348–363, Jan. 2008.

[2] C. S. Cho, B. M. Chung, and M. J. Park, "Development of real-time vision-based fabric inspection system," *IEEE Trans. Ind. Electron.*, vol. 52, no. 4, pp. 1073–1079, Aug. 2005.

[3] D.-M. Tsai and Y.-H. Tsai, "Defect detection in textured materials using color ring-projection correlation," *Mach. Vis. Appl.*, vol. 13, pp. 194–200, 2003.

[4] M. Al-Mouhamed, O. Toker, and A. Al-Harthy, "A 3-D vision-based man–machine interface for hand-controlled telerobot," *IEEE Trans. Ind. Electron.*, vol. 52, no. 1, pp. 306–319, Feb. 2005.

[5] Y. Motai and A. Kosaka, "Hand-eye calibration applied to viewpoint selection for robotic vision," *IEEE Trans. Ind. Electron.*, vol. 55, no. 10, pp. 3731–3741, Oct. 2008.

[6] Z. F. Yang and W. H. Tsai, "Viewing corridors as right parallelepipeds for vision-based vehicle localization," *IEEE Trans. Ind. Electron.*, vol. 46, no. 3, pp. 653–661, Jun. 1999.

[7] S. Segvic and S. Ribaric, "Determining the absolute orientation in a corridor using projective geometry and active vision," *IEEE Trans. Ind. Electron.*, vol. 48, no. 3, pp. 696–710, Jun. 2001.

[8] F. Wu, C. T. Lin, and Y. L. Chen, "Dynamic calibration and occlusion handling algorithms for lane tracking," *IEEE Trans. Ind. Electron.*, vol. 56, no. 5, pp. 1757–1773, May 2009.

[9] A. Broggi, M. Cellario, P. Lombardi, and M. Porta, "An evolutionary approach to visual sensing for vehicle navigation," *IEEE Trans. Ind. Electron.*, vol. 50, no. 1, pp. 18–29, Feb. 2003.

[10] T. Bucher *et al.*, "Image processing and behavior planning for intelligent vehicles," *IEEE Trans. Ind. Electron.*, vol. 50, no. 1, pp. 62–75, Feb. 2003.

[11] M. Al-Mouhamed, "A robust gross-to-fine pattern recognition system," *IEEE Trans. Ind. Electron.*, vol. 48, no. 6, pp. 1226–1237, Dec. 2001.

[12] P. Y. Hsiao, C. L. Lu, and L. C. Fu, "Multilayered image processing for multiscale Harris corner detection in digital realization," *IEEE Trans. Ind. Electron.*, vol. 57, no. 5, pp. 1799–1805, May 2010.

[13] M. Tistarelli and G. Sandini, "Dynamic aspects in active vision," *CVGIP Image Understand.*, vol. 56, no. 1, pp. 108–129, 1992.

[14] Y. Y. Tang, H. D. Cheng, and C. Y. Suen, "Transformation-ring-projection (TRP) algorithm and its VLSI implementation," *Int. J. Pattern Recognit. Artif. Intell.*, vol. 5, no. 1–2, pp. 25–56, 1991.

[15] Y. Y. Tang, H. Ma, J. Liu, B. Li, and D. Xi, "Multiresolution analysis in extraction of reference lines from documents with graylevel background," *IEEE Trans. Pattern Anal. Mach. Intell.*, vol. 19, no. 8, pp. 921–926, Aug. 1997.

[16] M.-S. Choi and W.-Y. Kim, "A novel two stage template matching method for rotation and illumination invariance," *Pattern Recognit.*, vol. 35, pp. 119–129, 2002.

[17] Y.-H. Lin and C.-H. Chen, "Template matching using the parametric template vector with translation, rotation and scale invariance," *Pattern Recognit.*, vol. 41, pp. 2413–2421, 2008.

[18] R. L. Kashyap and A. Khotanzad, "A model-based method for rotation invariant texture classification," *IEEE Trans. Pattern Anal. Mach. Intell.*, vol. 8, no. 4, pp. 472–481, Jul. 1986.

[19] H. Y. Kim and S. A. Araujo, "Grayscale template-matching invariant to rotation, scale, translation, brightness and contrast," in *Proc. Pac. Rim Symp. Image Video Technol.*, Santiago, Chile, 2007, pp. 100–113.

[20] M. Amiri and H.R. Rabiee, "A novel rotation/scale invariant template matching algorithm using weighted adaptive lifting scheme transform," *Pattern Recognit.*, vol. 43, pp. 2485–2496, 2010.

[21] E. Elboher and M. Werman, "Asymmetric correlation: A noise robust similarity measure for template matching," *IEEE Trans. Image Process.*, vol. 22, no. 8, pp. 3062–3073, Aug. 2013.

[22] Y. Y. Tang, B. F. Li, H. Ma, and J. Liu, "Ring-projection-wavelet-fractal signatures: A novel approach to feature extraction," *IEEE Trans. Circuits Syst. II, Analog Digital Signal Process.*, vol. 45, no. 8, pp. 1130–1134, Aug. 1998.

[23] D.-M. Tsai and Y.-H. Tsai, "Rotation-invariant pattern matching with color ring-projection," *Pattern Recognit.*, vol. 35, pp. 131–141, 2002.

[24] P. C. Yuen, G. C. Feng, and Y. Y. Tang, "Printed Chinese character similarity measurement using ring projection and distance transform," *Int. J. Pattern Recognit. Artif. Intell.*, vol. 12, pp. 209–221, 1998.

[25] [Online]. Available: http://mathworld.wolfram.com/ArchimedeanSpiral.html, accessed on May 5, 2015.

[26] R. C. Gonzalez and R. E. Woods, *Digital Image Processing*. EnglewoodCliffs, NJ, USA: Prentice Hall, 2007.

[27] H. Y. Kim, "Rotation-discriminating template matching based on Fourier coefficients of radial projections with robustness to scaling and partial occlusion," *Pattern Recognit.*, vol. 43, pp. 859–872, 2010.

[28] H. Ballard, "Generalizing the Hough transform to detect arbitrary shapes," *Pattern Recognit.*, vol. 13, no. 2, pp. 111–222, 1981.

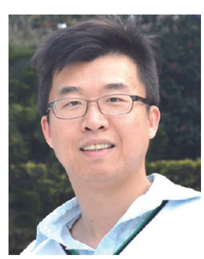

Huang-Chia Shih (M'08) received the B.S. degree (with highest honors) in electronic engineering from National Taipei University of Technology, Taipei, Taiwan, in 2000, and the M.S. and Ph.D. degrees in electrical engineering from National Tsing Hua University, Hsinchu, Taiwan, in 2002 and 2008, respectively.

He is an Associate Professor with the Department of Electronic Engineering, Yuan Ze University, Taoyuan, Taiwan. He served as a Visiting Scholar at the Department of Electronic Engineering, The University of Washington, Seattle, WA, USA, from September 2006 to April 2007, and a Visiting Professor at John von Neumann Faculty of Informatics, Obuda University, Budapest, Hungary, from July 2011 to September 2011. He has authored more than 50 technical papers published in refereed journals and conference proceedings. His research interests include content-based multimedia processing, pattern recognition, and human–computer interaction (HCI).

Dr. Shih has served as a Program Committee Member and Reviewer for international journals and conferences. He was the recipient of the Young Scholar Research Award from the Yuan Ze University, the Outstanding Youth Electrical Engineer Award from the Chinese Institute of Electrical Engineering in 2015, the Kwoh-Ting Li Young Researcher Award from the ACM Taipei/Taiwan Chapter in 2014, the Pan Wen Yuan Exploration Research Award from the Pan Wen Foundation in 2013, and the Best Paper Award from the International Symposium on Consumer Electronics (ISCE) 2013 and the Global Conference on Consumer Electronics (GCCE) 2015.

Kuan-Chun Yu received the B.E. degree in signal processing and image communication from the Department of Electrical Engineering, Yuan Ze University, Taoyuan, Taiwan, in 2013. He is currently working toward the Master's degree in the Department of Electrical Engineering, National Taiwan University of Technology, Taipei, Taiwan.

His research interests include image processing, pattern recognition, VLSI design, and video coding techniques.